JOURNAL OF SOLID STATE CHEMISTRY 92, 191–201 (1991)

Structure Defects in Rare-Earth–Iron Carbides with the Hexagonal Th_2Ni_{17} Structure Type: A Study by Means of High Resolution Electron Microscopy

W. COENE, F. HAKKENS, T. H. JACOBS,* AND K. H. J. BUSCHOW*

Philips Research Laboratories, P.O. Box 80.000, 5600 JA Eindhoven, The Netherlands

Received September 19, 1990

Rare-earth iron carbides $(RE)_2Fe_{17}C_x$ have the hexagonal ($hP38$) Th_2Ni_{17} structure from terbium to lutetium and for yttrium, provided that the carbon concentration is below the value of the hexagonal-to-rhombohedral transformation point. High resolution electron microscopy reveals structure defects which change the site symmetry and therefore the magnetocrystalline anisotropy of the rare-earth sublattice on a local scale. Under suitably chosen imaging conditions, the rare-earth atom columns can be identified as white dots in the high resolution images. Less bright or even absent dots at some particular positions of the rare-earth columns are interpreted in terms of partially disordered atom columns with a mixed occupation of rare-earth atoms and iron dumbbells. Image simulations confirm this hypothesis of local disorder. Conservative antiphase boundaries are observed. Defect areas containing successive nonconservative antiphase boundaries are identified as local slabs of material with the $ThMn_{12}$ structure type. © 1991 Academic Press, Inc.

Introduction

Recently, the magnetic and crystallographic properties of the iron-rich rare-earth (RE) intermetallic compounds $RE_2Fe_{17}C_x$ have been studied extensively (*1–4*) due to the potential application of these materials as permanent magnets. In a previous study (*5*), we have investigated by means of high resolution electron microscopy (HREM) the planar crystal defects in magnetic material of the type $Y_2Fe_{17}C_x$ ($x \geq 0.6$), which has the rhombohedral ($hR19$) Th_2Zn_{17} type of structure (space group $R\bar{3}m$). The crystal defects in these materials change the site symmetry of the RE atoms on a local scale. Due to the correlation between the site symmetry and the magnetic anisotropy at the RE atoms (*6*), local areas with different magnetic anisotropy are created at the defects. These anisotropy variations can affect the coercivity mechanism of these magnets.

In this paper, we focus our attention on the crystal defects in the $RE_2Fe_{17}C_x$ compounds, which have the hexagonal Th_2Ni_{17} type of structure (space group $P6_3/mmc$). Both the hexagonal Th_2Ni_{17} and the rhombohedral Th_2Zn_{17} structure types are superstructures of the $CaCu_5$ type of structure (space group $P6/mmm$). These three structures are layered structures built up of close-packed Fe-layers alternated by mixed RE–Fe layers. The $(RE)_2Fe_{17}$ superstruc-

* Also at Kamerlingh Onnes Laboratorium, P.O. Box 9504, 2300 RA Leiden, The Netherlands.

0022-4596/91 $3.00

Copyright © 1991 by Academic Press, Inc.
All rights of reproduction in any form reserved.

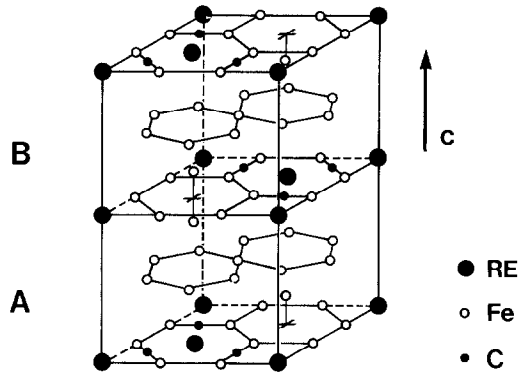

FIG. 1. Schematic representation of the hexagonal Th_2Ni_{17} structure type for $(RE)_2Fe_{17}C_x$ compounds. The carbon atoms in $RE_2Fe_{17}C_x$ fully occupy the interstitial positions in the figure, corresponding to $x = 3$.

tures can be derived from the $(RE)Fe_5$ structure by substituting one-third of all *RE* atoms in the mixed *RE*–Fe layers by Fe_2 dumbbells. The Fe_2 dumbbells have their axis along the *c*-direction, i.e., normal to the basal hexagonal (001) plane of the mixed *RE*–Fe layers. Three different layer types can be distinguished (A, B, and C) depending on the position of the Fe_2 dumbbell in the (001) plane. For the rhombohedral (*hR*19) Th_2Zn_{17} structure type, the stacking sequence along the *c*-axis is then given by ABCABC. The hexagonal (*hP*38) Th_2Ni_{17} structure type, which is shown in Fig. 1, is obtained in the case of the stacking sequence ABAB. Note that in Fig. 1, for a clearer appearance of the perspective drawing, the *c*-axis has been enlarged as compared to the real situation. Neutron diffraction experiments (*7*) have shown that the C atoms occupy interstitial hole sites in the mixed *RE*–Fe (001) planes, as indicated in Fig. 1. In the hexagonal structure, the *RE* atoms have a $D_{3h}(I)$ or $D_{3h}(II)$ site symmetry, depending on whether there are two *RE* atoms or two Fe_2 dumbbells at the neighboring positions along the *c*-axis. The symmetry symbols shown here are those used by Allen *et al.* (*6*). On the other hand, the *RE* atoms in the rhombohedral structure all have a C_{3v} site symmetry, i.e., with one *RE* atom and one Fe_2 dumbbell as neighbors along the *c*-axis.

In the pure $(RE)_2Fe_{17}$ ($x = 0$) compounds, the rhombohedral Th_2Zn_{17} structure is found in the lanthanide series from cerium to gadolinium (*8*). From terbium to lutetium, and for yttrium, the $(RE)_2Fe_{17}$ compounds have the hexagonal Th_2Ni_{17} structure. The $(RE)_2Fe_{17}C_x$ carbides ($x \neq 0$) have the same structure as the pure compounds ($x = 0$), with the exception of a carbon-induced structural transformation from the hexagonal to the rhombohedral type when the pure compound exhibits the hexagonal structure (*3*, *4*). The transition point x_t of this structural transformation is dependent on the *RE* atom: e.g., for thulium $x_t = 1.6$, for yttrium $x_t = 0.6$.

Experimental Methods

We have examined the hexagonal compounds Lu_2Fe_{17}, $Y_2Fe_{17}C_{x=0.4}$ and $Tm_2Fe_{17}C_{x-1.0}$. The materials were prepared by arc melting. Homogenization was achieved by annealing the alloys for a period of 2 to 3 weeks at a temperature of 1100, 900, and 1150°C, respectively. After annealing, the samples were quenched in water. Using X-ray powder diffraction, the samples turned out to be almost of single phase, with a small amount of elemental iron.

Thin specimens for HREM were prepared by ion beam milling at 5 kV until perforation, followed by a second milling step at 1.5 kV for a few hours, in order to minimize the "damage" produced during ion bombardment. Compared with the rhombohedral $Y_2Fe_{17}C_x$ ($x \geq 0.6$) compounds, which have been studied in (*5*), the hexagonal materials are much more subject to the ion milling damage. TEM specimens with the highest obtainable quality, i.e., with the thinnest amorphous layer and with the largest areas useful for HREM, were obtained for

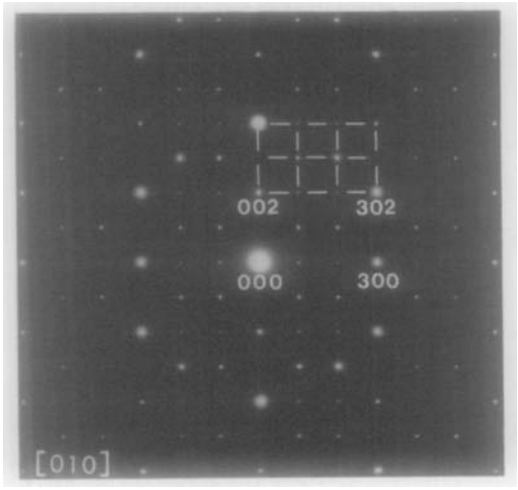

FIG. 2. Electron diffraction pattern of hexagonal $(RE)_2Fe_{17}C_x$ in [010] orientation.

$Tm_2Fe_{17}C_{x=1.0}$. We attribute this effect to the higher amount of carbon in the latter material, which yields less brittle samples.

High resolution structure imaging was performed at a Philips CM30/Super Twin electron microscope at 300 kV, with spherical aberration C_s = 1.15 mm. We have carried out the HREM observations in the mutually equivalent [100] or [010] orientation. The corresponding electron diffraction pattern is shown in Fig. 2. As can be seen from the [100] projection of the perfect hexagonal structure, which is shown in Fig. 3, homogeneous columns either of *RE* atoms or of Fe_2 dumbbells are then present along the electron beam direction. No *RE*/Fe_2 mixing occurs along the columns, and the hexagonal AB stacking sequence can be derived directly from the [100] projection.

Conservative Antiphase Boundaries

Conservative antiphase boundaries (APBs) in the hexagonal $(RE)_2Fe_{17}C_x$ compounds have a (001) habit plane with a displacement vector $\mathbf{R} = \pm\frac{1}{3}[1\bar{1}0]$. These defects do not change the 2 : 17 composition of the material. When crossing the APB plane, the ABAB stacking sequence changes either into CBCB, or into ACAC. The former situation yields:

$$\begin{array}{c}\\ \\ \text{A B A B A B C B C B C B}\\ \\ \\ \end{array}$$

At the APB plane, a triplet of rhombohedral stacking (ABC) is formed. The *RE* atoms in the middle of the rhombohedral triplet have the C_{3v} site symmetry: they have one *RE* atom and one Fe_2 dumbbell as neighbors.

Figure 4 shows a HREM image of a conservative APB in [100] oriented $Tm_2Fe_{17}C_{x=1.0}$. The focus condition of the microscope is chosen in such a way that only the *RE* columns are imaged as white dots. The hexagonal ABAB superstructure is then readily derived from the HREM image. The correspondence between structural features and the observed image contrast has been obtained on the basis of HREM image simulations using the electron-optical parameters of the CM30 microscope. For ultrathin specimen foils ($t \leq 3$ nm), the superstructure is imaged at a focus setting slightly above Scherzer focus, i.e., $\Delta f \approx -70$ nm to -90 nm. The thickness of the specimens we used for HREM is estimated to be slightly greater. For these specimen foils (3 nm $\leq t \leq$ 10 nm), HREM image simulations show that the focus condition for superstructure imaging is in the range $\Delta f \approx -10$ nm to -40 nm. The optimum focus for the latter thickness range is around $\Delta f \approx -30$ nm. In order to see the shift in the hexagonal stacking sequence at the APB more clearly, it is advisable to look at the HREM image of Fig. 4 under grazing incidence along the *c*-direction. In the structure projection of Fig. 3, three different types of *RE*/Fe_2 atom rows along the *c*-axis can be distinguished. The first type of row consists of only *RE* atoms along the *c*-axis. The other types of rows are built up of alternating *RE*

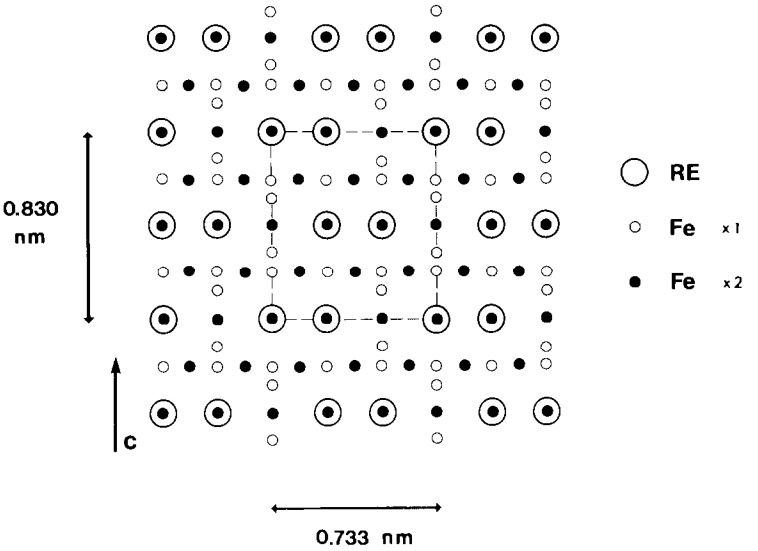

FIG. 3. [100] projection of the hexagonal structure of $RE_2Fe_{17}C_x$ with omission of C atoms. Filled circles indicate two successive Fe atoms along the axis of projection. The parameters of the unit cell in projection as indicated hold for the case RE = Y and x = 0.

atoms and Fe_2 dumbbells and are mutually shifted over a distance of $c/2$. The former type of rows consisting of *RE* atoms only are recognized in the HREM image (Fig. 4) by white dots that are closely spaced along the c-axis. These rows of closely spaced white dots are clearly revealed when looking under grazing incidence along the c-axis. Going further from the bottom to the top part of Fig. 4, the shift of $\frac{1}{3}$ $[1\bar{1}0]$ to the left at the APB area becomes obvious. When the respective stacking sequences (AB and AC) around the APB are observed more closely, one can see that some white dots at the *RE* positions are less bright, or may even be absent. This phenomenon is also frequently observed in the bulk hexagonal structure, and will be discussed in the next section. Therefore, a single APB defect plane, imaged in edge-on orientation, can hardly be distinguished in the HREM image of Fig. 4. Presently, the effect of the weakening of some of the white dots in the APB area is attributed to local substitutional disorder of *RE* atoms and Fe_2 dumbbells, yielding a mixed RE/Fe_2 column along the electron beam direction. On the other hand, the assumption of an inclined APB plane, which yields a coincidence pattern between the ABAB and ACAC stacking sequences, cannot be completely disregarded.

Local Disorder: Mixed RE/Fe_2 Columns

In Fig. 5, a HREM image is shown of a [100]-oriented grain of the hexagonal $Tm_2Fe_{17}C_{x=1.0}$ compound. The sample area shown in Fig. 5 does not contain any planar crystal defects, but clear variations in the brightness of the individual white dots at the *RE* positions can be observed. Similar effects have been reported in Au–Mn (*9, 10*) and in Pt–V (*11*) binary alloy systems; these effects were explained by the presence of partially disordered or mixed atomic columns, i.e., by deviations from the ideal homogeneous composition along a particular atom column. A theoretical investigation

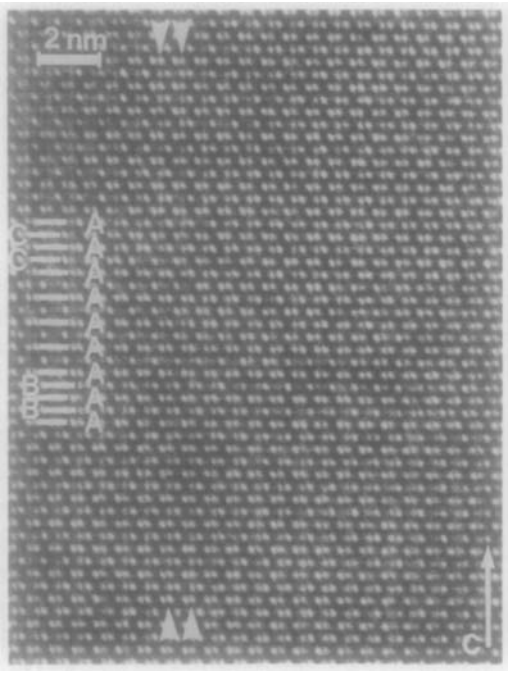

FIG. 4. [100] HREM image of a conservative antiphase boundary in $Tm_2Fe_{17}C_{x=1.0}$. The stacking sequences at the defect area are indicated.

(*12*) has shown that for thin foils a quasi-monotonic relation is found between the composition of the mixed column and the HREM image contrast at the position of that column; distribution effects along a mixed column only become significant for thicker foils. Recently, different algorithms have been devised (*13*) in order to obtain a quantitative measure for the concentration of a mixed column, and they were evaluated (*13*) on simulated HREM images of $Al_xGa_{1-x}As$.

The weakening or extinction of the white dots in Fig. 5 is explained in a similar way by mixed *RE*/Fe_2 columns. The situation is slightly more complicated since the Fe_2 "atom" has a dumbbell axis of about 0.24 nm. Therefore, a succession of two Fe_2 dumbbells, adjacent to each other along the *c*-axis, is much less likely to occur. Indeed, in that case the top and bottom Fe atoms of the successive dumbbells would be separated by a distance of about 0.18 nm, which is much smaller than the dumbbell axis of 0.24 nm. Due to these size considerations, only the *RE* atoms with the $D_{3h}(I)$ site symmetry (along *c*, two *RE* neighbors) can be substituted by Fe_2 dumbbells. This substitution mechanism leads to the generation of mixed *RE*/Fe_2 columns along the [100] viewing direction in the hexagonal structure. Due to such a *RE*–Fe_2 substitution, the site symmetry of the neighboring *RE* atoms changes from $D_{3h}(I)$ into a C_{3v}-like site symmetry with one *RE* and one Fe_2 neighbor. The

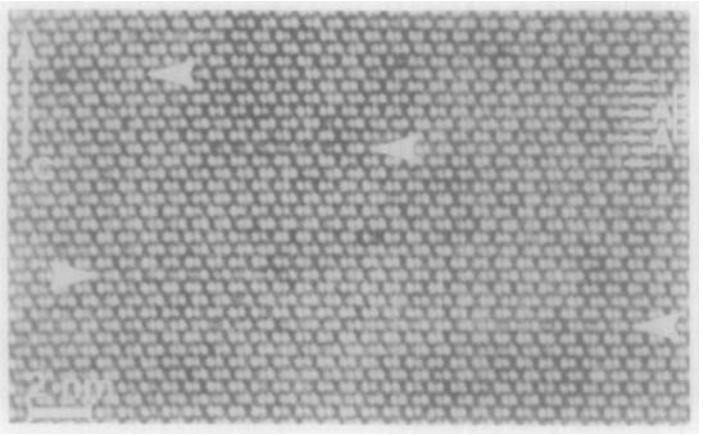

FIG. 5. [100] HREM image of mixed *RE*/Fe_2 columns in $Tm_2Fe_{17}C_{x=1.0}$. The partially disordered columns are represented by less bright or absent white dots.

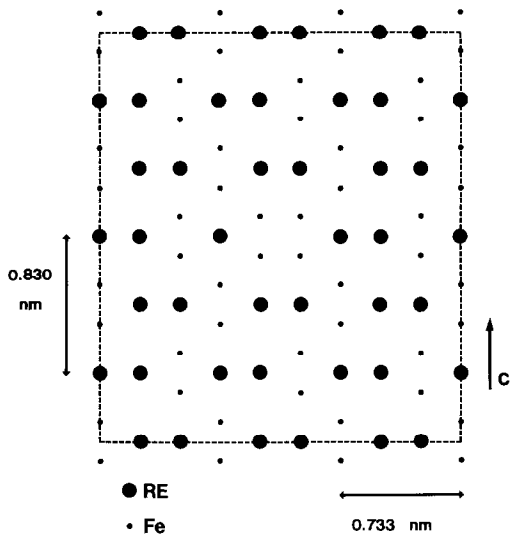

FIG. 6. [100] Geometrical model for the supercell used in the HREM image simulations of the mixed RE/Fe_2 column in $(RE)_2Fe_{17}C_x$ compounds. Only *RE* atoms and Fe_2 dumbbells are drawn; the remaining Fe framework is omitted. Note the substitution of the central *RE* atom by an Fe_2 dumbbell.

HREM image in Fig. 5 confirms that the partially disordered or mixed atom columns only occur at the *RE* position with the $D_{3h}(I)$ site symmetry. In the iron-rich lutetium system, Givord, Lemaire, and coworkers (*14*) have explained their X-ray and neutron diffraction experiments in terms of disordered substitutions of this type.

A confirmation of the observed effects is obtained by means of HREM image simulations of mixed RE/Fe_2 columns. We have used the real space program (*15*) for the dynamical electron diffraction calculations at 300 kV in the case of a supercell of 2.20 nm × 2.48 nm, in which the central *RE* atom (with $D_{3h}(I)$ site symmetry) can be replaced by an Fe_2 dumbbell (see Fig. 6 for the model of the supercell in [100] projection). The substituted Fe_2 dumbbells are positioned as a continuous string in the center of the foil. Indeed, the experimental foil thicknesses are thin enough ($t \leq 10$ nm) so that distribution effects of the atoms along the mixed column have no significance. The electron-optical parameters used in the HREM image calculations for the CM30 microscope are: spherical aberration $C_s = 1.15$ mm, defocus spread $\Delta = 8.0$ nm, half angle of beam convergence $\alpha = 1.2\ 10^{-3}$ rad. Figure 7 shows simulated HREM images for foil thicknesses $t = 4.2$ nm (5 atoms in a column) and $t = 9.3$ nm (11 atoms in a column). Only the simulated images for $\Delta f = -30$ nm are shown: this is the optimum focus condition for the imaging of the superstructure in that thickness range. The Fe_2 content of the central *RE* column is varied between 0 and 100% as indicated. The simulated images reveal that the brightness of the white dot at the position of the mixed column diminishes roughly in a monotonic way with the Fe_2 content of the column. Note that for the thicker specimen foils ($t \geq 9$ nm), the white dots in the image at the pure RE–$D_{3h}(I)$ columns (0% Fe_2) are slightly less bright than the dots at the RE–$D_{3h}(II)$ columns. This is obviously not a composition effect, but the different image features revealing the differences in site symmetry are due to dynamical diffraction effects between atom columns, which become more important with increasing foil thickness. Note also that the weakening of the white dot with increasing Fe_2 content proceeds faster for the thin sample ($t = 4.2$ nm) as compared to the somewhat thicker sample ($t = 9.3$ nm). For the latter case, a fairly high (≥50%) Fe_2 concentration is needed in order to observe the weakening of the white dot.

As stated above, the RE–Fe_2 substitutions only occur at *RE* atoms with a $D_{3h}(I)$ site symmetry. In the rhombohedral $(RE)_2Fe_{17}C_x$ compounds, these local substitutions have not been observed (*5*). Indeed, the C_{3v} site symmetry of the *RE* atoms in the perfect rhombohedral structure implies one Fe_2 dumbbell as a neighbor along the *c*-axis, not leaving enough free space for a RE–Fe_2 substitution. However, the situation is different at the conservative APBs of the rhombohedral structure, with respective stacking sequences ABCABABC and

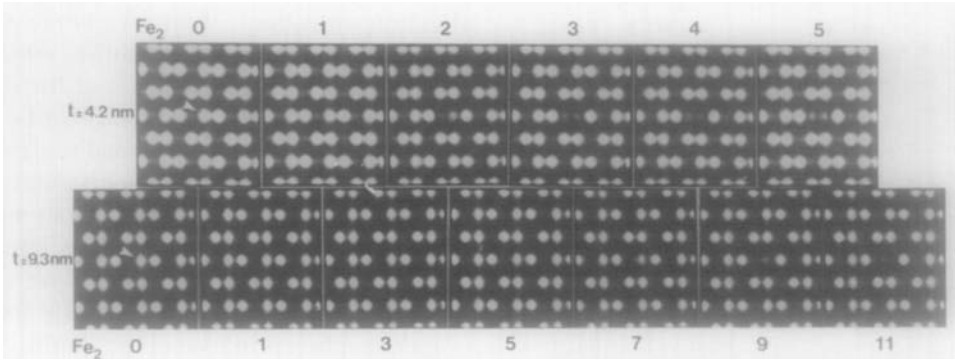

FIG. 7. HREM image simulations for a mixed RE/Fe_2 column in hexagonal $Tm_2Fe_{17}C_x$ in [100] orientation. The optimum defocus setting is chosen ($\Delta f = -30$ nm). The foil thickness t and the number of Fe_2 dumbbells of the mixed column are indicated. The white dot at the position of the disordered column is arrowed.

ABCACBCABC for the intrinsic and extrinsic faults. Local slabs with hexagonal stacking sequence are formed at the APBs, with a mixed $D_{3h}(I)$–$D_{3h}(II)$ site symmetry. At the former positions, mixed RE/Fe_2 columns can be obtained in the rhombohedral compounds as shown in the HREM image of Fig. 8 for the case of an extrinsic fault. Note that due to the disordered RE/Fe_2 columns, the 2 : 17 composition of the matrix is indeed locally changed at the originally conservative APB. Again, extensive image simulations for mixed columns at the conservative APBs prove the validity of our interpretation. A selection of simulated images for the extrinsic case is shown in Fig. 9: the Fe_2 concentrations of the $D_{3h}(I)$ RE columns at the A and B planes, left and right of the APB plane at C, are taken identical to each other and are further homogeneous along the (001) planes.

For the hexagonal compounds, the substitution by Fe_2 dumbbells occurs sometimes in a quasiperiodic manner over a larger specimen area. Such an area can be observed in the HREM image of Fig. 10, showing (001) planes with alternatingly single (A) and paired (B) white dots. In this case, nearly all atoms in the RE–$D_{3h}(I)$ columns of every B plane in the ABAB sequence are substituted by Fe_2 dumbbells. In the limit of a 100% periodic substitution by an Fe_2 dumbbell of one of

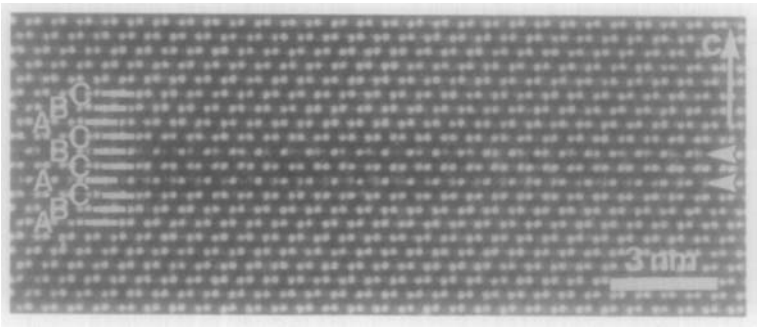

FIG. 8. [100] HREM image of mixed RE/Fe_2 columns at a conservative APB (extrinsic fault) in rhombohedral $Y_2Fe_{17}C_{x=0,9}$. The partially disordered columns are represented by less bright or absent white dots: they appear only at the A and B plane (indicated by arrows) just below and above the APB plane at C.

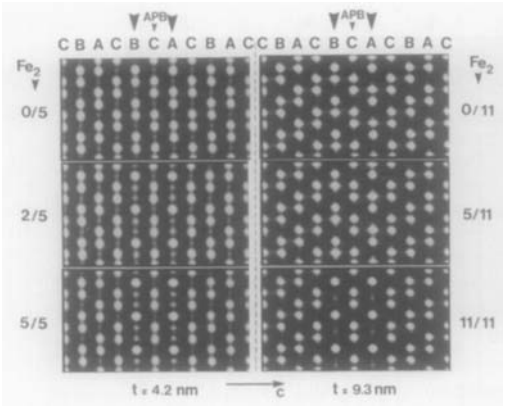

FIG. 9. HREM image simulations for mixed Y/Fe_2 columns at a conservative APB (extrinsic fault) in rhombohedral $Y_2Fe_{17}C_x$ in [100] orientation. The optimum defocus setting ($\Delta f = -30$ nm) is chosen. The foil thickness t and the Fe_2 content of the mixed columns are indicated.

the two RE–$D_{3h}(I)$ positions in the hexagonal $(RE)_2Fe_{17}$ unit cell, an Fe-rich $(RE)_1Fe_{12}$ phase is obtained, with a unit cell in [100] projection as shown in Fig. 11. Then, in that ultimate case, only RE atoms with a $D_{3h}(II)$-like site symmetry are present.

Nonconservative Antiphase Boundaries—Inclusions of $(RE)_1Fe_{12}$ Phase

Nonconservative APBs with a (100) habit plane and with a displacement vector $\mathbf{R} = \frac{1}{3}[1\bar{1}0]$ are observed. These APBs are characterized by the withdrawal of a (100) plane, which contains only RE atoms and no Fe_2 dumbbells. The HREM image in Fig. 12 is typical: in all cases two successive nonconservative APBs are present. This phenomenon is identified by the presence of two single zigzag lines of white dots (or RE columns) in between the paired zigzag lines of dots of the perfect hexagonal structure. A schematic diagram of the defect area is shown in Fig. 13. The defect area has an equal concentration of RE atoms and Fe_2 dumbbells and is therefore more Fe-rich than the $(RE)_2Fe_{17}$ structure types ($\frac{2}{3}$ RE–$\frac{1}{3}$ Fe_2 concentration). With 5 Fe atoms in the basic Fe framework for each Fe_2 dumbbell or RE atom, the composition of the defect area amounts to $(RE)_1Fe_5(Fe_2)_1Fe_5 = (RE)_1Fe_{12}$. A three-dimensional representation of the 2 : 17 and 1 : 12 superstructures is shown in Fig. 14 (again, only RE atoms and Fe_2 dumbbells are drawn). The interface plane between both structure types is the (100) hexagonal plane. The locally formed superstructure is indeed of the $ThMn_{12}$ type, if one neglects a tetragonal-to-orthorhombic deformation due to a small difference of about 2% between the c- and a-parameters of the hexagonal 2 : 17 superstructure. Recently, the magnetic properties of the pseudobinary compound $YFe_{12-x}Ti_x$ with the $ThMn_{12}$ structure have been studied (*16*) and explained in terms of the structural relationships among the 1 : 5, 2 : 17, and 1 : 12 structure types.

Discussion and Concluding Remarks

From the high resolution observations described in the preceding sections, it is obvi-

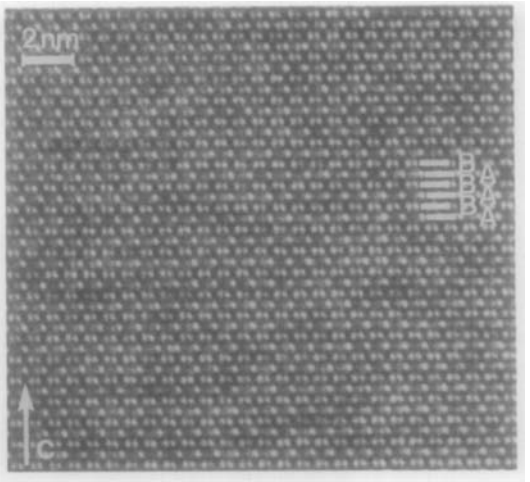

FIG. 10. HREM image of $Tm_2Fe_{17}C_{x=1.0}$ revealing a quasiperiodic substitution by Fe_2 dumbbells of nearly all RE atoms at the $D_{3h}(I)$ symmetry sites in every second plane in the hexagonal $ABAB$ stacking sequence. For a 100% substitution, a $(RE)_1Fe_{12}$ phase is obtained.

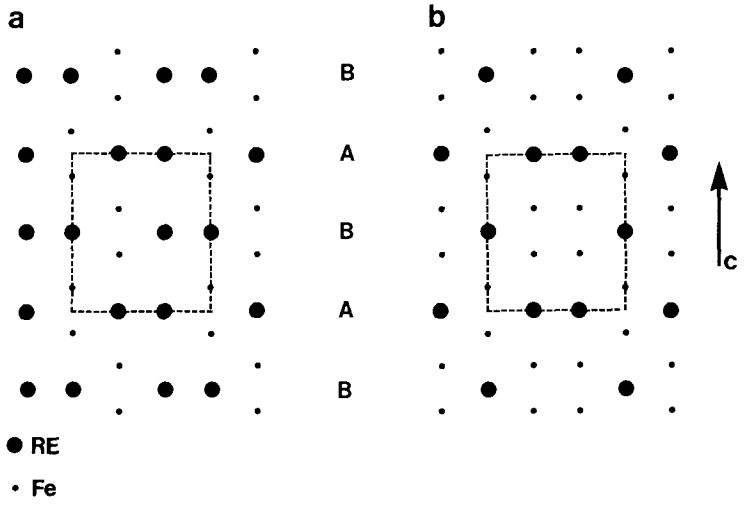

FIG. 11. [100] projection of (a) the hexagonal $(RE)_2Fe_{17}$ structure, and (b) the $(RE)_1Fe_{12}$ phase as obtained from the HREM image of Fig. 10. Only *RE* atoms and Fe_2 dumbbells are drawn.

ous that different types of structure defects (antiphase boundaries, partially disordered columns) occur in hexagonal $(RE)_2Fe_{17}C_x$ compounds, which give rise to *RE* atoms with a C_{3v} or C_{3v}-like site symmetry, which is associated to the ideal rhombohedral $(RE)_2Fe_{17}$ lattice. The APB density in the hexagonal $(RE)_2Fe_{17}C_x$ compounds is markedly lower than in the rhombohedral $(RE)_2Fe_{17}C_x$ compounds (*5*), which have been prepared under identical experimental conditions (arc melting, annealing treatment). On the other hand, the hexagonal materials exhibit a high density of partially disordered or mixed RE/Fe_2 columns. Local

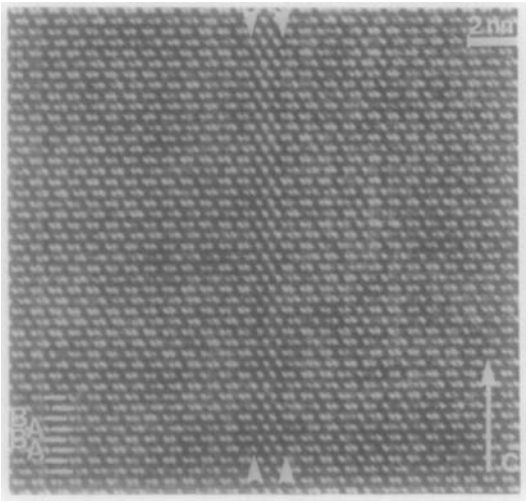

FIG. 12. [100] HREM image of nonconservative APBs in $Tm_2Fe_{17}C_{x=1.0}$. The two successive APBs represent a local slab consisting of two unit cells of the $(RE)_1Fe_{12}$ phase.

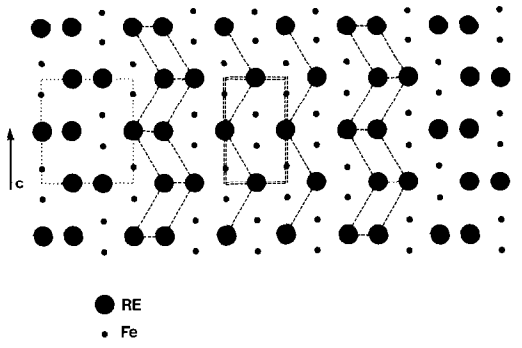

FIG. 13. Geometrical model of the succession of two nonconservative APBs in hexagonal $(RE)_2Fe_{17}C_x$ compounds in [100] orientation. Only *RE* atoms and Fe_2 dumbbells are drawn. The single and paired zigzag lines of *RE* atoms are indicated. The unit cell in [100] projection of the $(RE)_1Fe_{12}$ phase is outlined by the double-bar line; the projected unit cell of the hexagonal $(RE)_2Fe_{17}$ phase is indicated by the dotted line on the left.

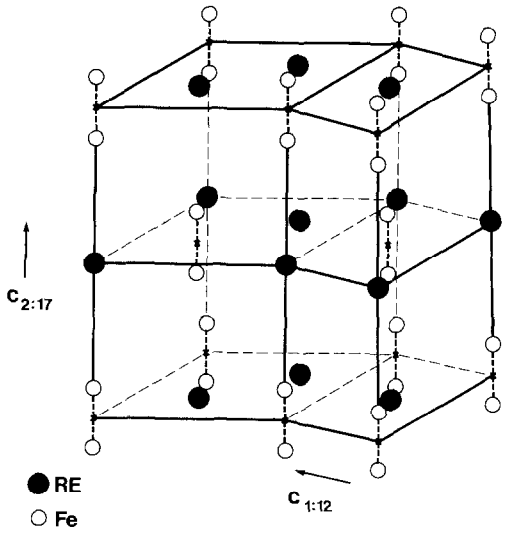

FIG. 14. Perspective representation of the structural coherence of the hexagonal $(RE)_2Fe_{17}$ phase (left) and the $(RE)_1Fe_{12}$ phase (right) with (100) interface plane. Only Fe_2 dumbbells and *RE* atoms are shown.

areas are also observed in which a quasiperiodic and nearly 100% substitution of Fe_2 dumbbells for the *RE* atoms at the $D_{3h}(I)$ sites leaves only *RE* positions with a $D_{3h}(II)$-like site symmetry. Due to size considerations, the formation of mixed RE/Fe_2 columns is highly unfavorable in the ideal rhombohedral lattice; experimentally, the partially disordered columns are only observed here at the conservative APBs of the rhombohedral compounds.

Nonconservative APBs in the hexagonal compounds are only observed in a twofold succession leading to the formation of local slabs with the $ThMn_{12}$ structure type. The pure $(RE)_1Fe_{12}$ compounds do not exist, but pseudobinary compounds $(RE)_1(Fe_{12-x}M_x)$ can be formed (see, e.g., (*16*, *17*)) with M = Ti, Al, W, Si . . . . In our case, the $(RE)_1Fe_{12}$ phase exists as a defect structure, with the $(RE)_1Fe_{12}$ slabs giving rise to a locally different magnetocrystalline anisotropy. For instance, in the case RE = Y, the overall in-plane anisotropy of Y_2Fe_{17} is changed into an easy-axis magnetization for YFe_{12} along the $c_{1:12}$-axis (*16*). The $c_{1:12}$-axis is parallel to $[110]_{2:17}$, and to $[100]_{1:5}$, with $c_{1:12} = a_{1:5}$.

A high density of mixed RE/Fe_2 columns and/or of $(RE)_1Fe_{12}$ slabs implies an increased concentration of Fe_2 dumbbells. This may be accompanied by an expansion of the lattice in the *c*-direction since the two Fe atoms in the Fe_2 dumbbell need more space along *c* than the replaced *RE* atom. The reverse argument holds in the basal hexagonal plane, implying a contraction of the *a*-parameter. This effect can be observed in the X-ray diagrams. In fact, Givord *et al.* (*14*) have obtained the very first experimental evidence for this type of disordered substitutions in the Th_2Ni_{17} structure, which we have reported in this paper, from structure determinations by X-ray and neutron diffraction.

Acknowledgment

The authors thank Dr. A. F. de Jong and Mr. D. B. de Mooij for stimulating discussions and useful suggestions.

References

1. D. B. DE MOOIJ AND K. H. J. BUSCHOW, *J. Less-Common Metals* **142,** 349 (1988).
2. P. C. M. GUBBENS, A. M. VAN DER KRAAN, T. H. JACOBS, AND K. H. J. BUSCHOW, *J. Magn. Magn. Mater.* **80,** 265 (1989).
3. W. COENE, F. HAKKENS, T. H. JACOBS, D. B. DE MOOIJ, AND K. H. J. BUSCHOW, *J. Less-Common Metals* **157,** 255 (1990).
4. K. H. J. BUSCHOW, T. H. JACOBS, AND W. COENE, *Proc. Intermag, IEEE Trans. Magn.* **26,** 1364 (1990).
5. W. COENE, F. HAKKENS, T. H. JACOBS, AND K. H. J. BUSCHOW, *Philos. Mag.* (1991), in press.
6. C. W. ALLEN, D. L. KURUZAR, AND A. E. MILLER, *IEEE Trans. Magn.* **MAG-10,** 716 (1974).
7. R. B. HELMHOLDT AND K. H. J. BUSCHOW, *J. Less-Common Metals* **155,** 15 (1989).
8. K. H. J. BUSCHOW, *Rep. Prog. Phys.* **40,** 1179 (1977).
9. D. SHINDO, K. HIRAGA, AND M. HIRABAYASHI, *Sci. Rep. Ritu Ser. A* **32,** 32 (1984).

10. O. TERASAKI, D. J. SMITH, AND G. J. WOOD, *Acta Crystallogr. B* **42,** 39 (1986).

11. D. SCHRIJVERS AND S. AMELINCKX, *Acta Metall.* **34,** 43 (1986).

12. W. COENE, D. VAN DYCK, J. VAN LANDUYT, AND S. AMELINCKX, *Philos. Mag. B* **56,** 415 (1987).

13. A. F. DE JONG AND D. VAN DYCK, *Ultramicroscopy* **33,** 269 (1990).

14. D. GIVORD, R. LEMAIRE, J. M. MOREAU, AND E. ROUDAUT, *J. Less-Common Metals* **29,** 361 (1972).

15. W. COENE AND D. VAN DYCK, *Ultramicroscopy* **15,** 287 (1984).

16. BO-PING HU, HONG-SHUO LI, AND J. M. D. COEY, *J. Appl. Phys.* **67,** 4838 (1990).

17. K. H. J. BUSCHOW, D. B. DE MOOIJ, M. BROUHA, H. H. A. SMIT, AND R. C. THIEL, *IEEE Trans. Magn.* **MAG-24,** 1161 (1988).